

Magnetic Ordering and Crystal Field Effects in Quasi Caged Structure Compound PrFe_2Al_8

Harikrishnan S. Nair,^{1,*} Sarit K. Ghosh,¹ Ramesh Kumar K.,¹ and André M. Strydom¹

¹Highly Correlated Matter Research Group, Physics Department,
P. O. Box 524, University of Johannesburg, Auckland Park 2006, South Africa
(Dated: August 22, 2018)

The compound PrFe_2Al_8 possesses a three-dimensional network structure resulting from the packing of Al polyhedra centered at the transition metal element Fe and the rare earth Pr. Along the c -axis, Fe and Pr form *chains* which are separated from each other by the Al-network. In this paper, the magnetism and crystalline electric field effects in PrFe_2Al_8 are investigated through the analysis of magnetization and specific heat data. A magnetic phase transition in the Pr lattice is identified at $T_N^{\text{Pr}} \approx 4$ K in dc magnetization and ac susceptibility data. At 2 K, the magnetization isotherm presents a ferromagnetic saturation, however, failing to reach full spin-only ferromagnetic moment of Pr^{3+} . Metamagnetic step-like low-field features are present in the magnetization curve at 2 K which is shown to shift upon field-cooling the material. Arrott plots centered around T_N^{Pr} display "S"-like features suggestive of an inhomogeneous magnetic state. The magnetic entropy, S_m , estimated from specific heat outputs a value of $R \ln(2)$ at T_{N2} suggesting a doublet state for Pr^{3+} . The magnetic specific heat is modeled by using a 9-level Schottky equation pertinent to the Pr^{3+} ion with $J = 4$. Given the crystalline electric field situation of Pr^{3+} , the inference of a doublet state from specific heat and consequent long-range magnetic order is an unexpected result.

PACS numbers:

I. INTRODUCTION

Intermetallic alloys of the 1:2:8 composition, RT_2X_8 , possess quasi cage structures consisting of polyhedra that cover the rare earth and the transition metal. These structural peculiarities of cage-like structures are interesting from the perspective of thermoelectric properties[1] for realizing high thermoelectric power. For example, a positive maximum of $20 \mu\text{V}/\text{K}$ was observed for CeFe_2Al_8 at 150 K. However, limited work on such compounds and the lack of complete understanding of the observed magnetic properties are compelling reasons to investigate new compounds in RT_2X_8 or to re-investigate some of the reported ones. The RT_2X_8 compounds crystallize in orthorhombic space group $Pbam$ (#55) [2]. In this space group, there are four formula units in the unit cell with one Wyckoff position ($4g$) for the R atom, two ($4g$) for T and nine ($2a$, $2d$, $4g$ and $4h$) for the X atom [2, 3]. The R or T atom in this structure is surrounded by nine to twelve X atoms. The R and the T atoms form a *chain* parallel to the c -axis which are separated by the X atoms. It is important to mention here a major question regarding the structural chemistry of 1:2:8 compounds regarding why they do not form 2:1:8 or 1:1:5 stoichiometries which are more stable, especially known for the Ce-variants[4]. It has been found from previous studies that the reason lies in the ionic size of the R and the X . In the case of 1:1:5 and 2:1:8-stoichiometries, the R -ion is in the trivalent f^1 (Ce) state whereas in 1:2:8 systems, the rare earth is in divalent or mixed-valent state [5]. In Ce-based 1:2:8 systems, [1, 6, 7] a transition from magnetic trivalent state of Ce to non-magnetic Kondo-like state of Ce is observed depending on the type of T and X atoms.

Strongly correlated electron behaviour was one of the fo-

cus themes to investigate the RT_2X_8 compounds and such signatures have been experimentally observed in CeT_2Al_8 [$T = \text{Fe}, \text{Co}$][7]. It was argued that the ground state of these compounds was governed by RKKY interaction[9] but possessed contrasting outcomes – in one case a metallic Fermi liquid state was evidenced whereas in the other, a heavy

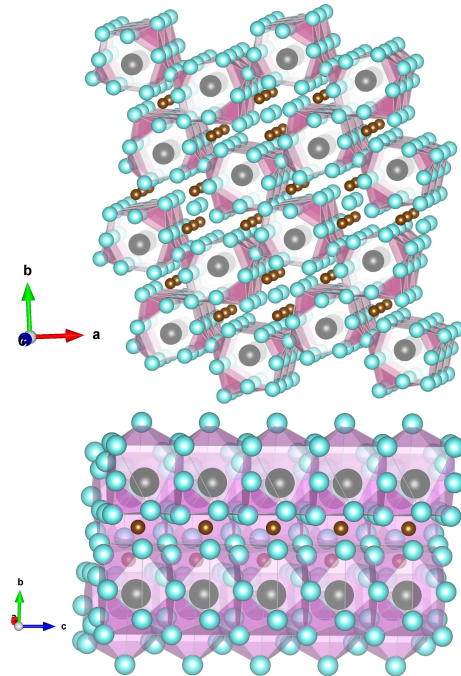


FIG. 1: *top*: A projection of the crystal structure of PrFe_2Al_8 along the c -axis showing the network of Al atoms (cyan) and the vacant space where Pr (black) and Fe (brown) form *chains* parallel to the c -axis. *bottom*: The view parallel to c -axis showing the chains of Pr. The figure was created using the software VESTA.[8]

*Electronic address: h.nair.kris@gmail.com, hsnair@uj.ac.za

TABLE I: The atomic positions of PrFe_2Al_8 in $Pbam$ space group. The refined lattice parameters are a (Å) = 12.5098(5), b (Å) = 14.4410(1), and c (Å) = 4.0401(7). The U_{iso} values were fixed to the values of PrCo_2Al_8 [11].

Atom	site	x	y	z	U_{iso}
Pr	4g	0.3394	0.3173	0.0	0.0029
Fe(1)	4g	0.1511	0.0951	0.0	0.0018
Fe(2)	4g	0.0291	0.3969	0.0	0.0021
Al(1)	2d	0.0000	0.5000	0.5	0.0033
Al(2)	2a	0.0000	0.0000	0.0	0.0053
Al(3)	4h	0.0264	0.1376	0.5	0.0053
Al(4)	4h	0.1627	0.3703	0.5	0.0031
Al(5)	4h	0.2313	0.1663	0.5	0.0035
Al(6)	4h	0.3389	0.4818	0.5	0.0034
Al(7)	4h	0.4598	0.1834	0.5	0.0028
Al(8)	4g	0.3347	0.0371	0.0	0.0041
Al(9)	4g	0.0953	0.2545	0.0	0.0043

Fermi-liquid with proximity to long-range magnetic order[7]. Cerium based RT_2X_8 with $X = \text{Al, Ga}$ have been reported previously also [1, 10] on which Mößbauer spectroscopy[1] and neutron diffraction studies[6] were performed in order to understand the magnetic ground state. Interestingly, no signature of long-range magnetic order was obtained in the case of CeFe_2Al_8 from neutron powder diffraction data though the magnetic susceptibility displayed a broad transition around 5 K [6]. Though Ce-based $RT_2\text{Al}_8$ were investigated in detail in the past, only a few reports on Pr-based systems exist. For example, PrCo_2Al_8 displays a phase transition at 5 K and metamagnetic-like steps in magnetic hysteresis[11]. From the analysis of high temperature magnetic susceptibility and estimates of effective paramagnetic moment, any contribution from Co magnetism was ruled out. The absence of magnetism of the T sub-lattice was a feature observed in the case of CeFe_2Al_8 also [7]. In the case of $\text{CeCo}_{2-x}\text{T}_x\text{Al}_8$ single crystals where doping at the Co-site was performed with $T = \text{Mn, Fe and Ni}$, only a slight enhancement of magnetic moment compared to the Ce^{3+} -only moment was observed[12]. It is, hence, interesting to investigate other compounds in the $RT_2\text{Al}_8$ class to probe the extent of magnetic ordering in the rare earth and transition metal lattices.

In the present paper we investigate the magnetism of the Pr-based RT_2X_8 compound PrFe_2Al_8 . Fig. 1 (top) shows the projection of the crystal structure on the ab -plane displaying the network of Al and the chain-like formation of Pr and Fe along the c -axis (bottom). These structural peculiarities certainly have a bearing on the magnetism of this class of compounds. The magnetism of Pr-based compounds can be strongly influenced by the crystal field levels of Pr^{3+} . Depending on whether the crystal field levels are comparable in energy scales with other interactions (especially magnetic), non-magnetic singlet or doublet crystal field ground states can result. To cite an example, the point charge model calculations for the Pr site in PrSi predicted the splitting of $J = 4$ Pr^{3+} ground state into 9 singlets thereby rendering spontaneous magnetic order impossible. However, an anomalous ferromagnetic ground state was experimentally unraveled

in PrSi[13]. Similarly, the point symmetry of the Pr-site in PrFe_2Al_8 is m (C_s) which predicts 9 distinct singlets from a 9-fold degenerate state and presupposes a non-magnetic

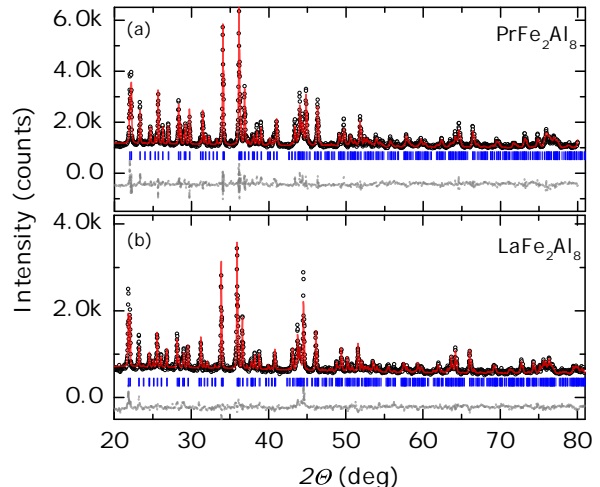


FIG. 2: The experimentally observed x ray powder diffraction pattern of PrFe_2Al_8 shown in black circles in (a). The red solid line is the Rietveld fit assuming $Pbam$ space group model. The vertical bars are the allowed Bragg peaks and the gray dotted line is the difference curve. For a comparison, the x ray diffraction pattern of the isostructural compound LaFe_2Al_8 is presented in (b) along with the results of Rietveld refinement.

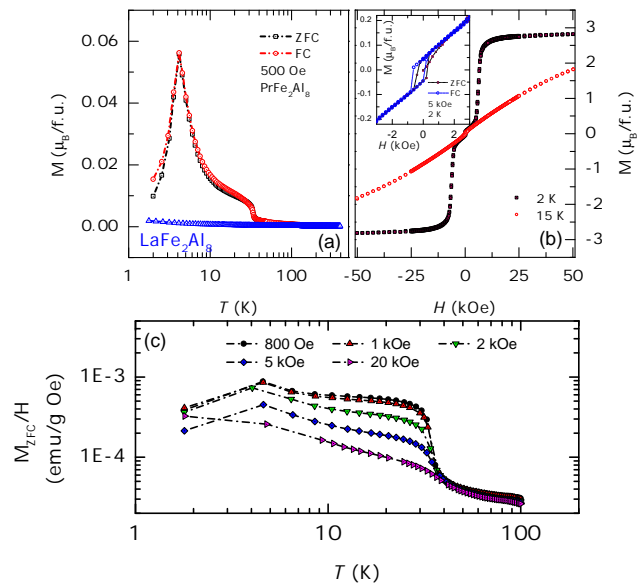


FIG. 3: The magnetization curves of PrFe_2Al_8 in ZFC and FC modes are shown in (a). Two transitions at $T_{anom} \approx 34$ K and at $T_N^{Pr} \approx 4$ K are observed. The magnetization curve of LaFe_2Al_8 is also presented for a comparison. (b) Shows the magnetic hysteresis at 2 K and at 15 K. Step-like features are observed in the low-field region at 2 K shown magnified in the inset. The inset also present field-cooled data exhibiting an exchange bias-like shift. (c) Displays M_{ZFC}/H at different applied fields 800 Oe to 20 kOe. The transition at T_{N2} is suppressed at 10 kOe while that at T_{anom} appears very robust.

TABLE II: The interatomic distances in PrFe_2Al_8 compared with those in LaFe_2Al_8 . The structures of both the compounds were refined in $Pbam$ space group. The distances given in the table are in the units of Angstrom (\AA). In all cases, a range of distances are indicated which is due to the quasi-caged structure of these compounds. The Pr-Pr distance along the c -axis is given in the table. Along a and b , the Pr-Pr distances vary in the range of 6.5 to 7.5 \AA .

PrFe_2Al_8	LaFe_2Al_8
Pr-Pr: 4.04	La-La: 4.06
Fe(1)-Fe(1): 4.04 – 6.18	Fe(1)-Fe(1): 4.06 – 6.21
Fe(2)-Fe(2): 3.06 – 4.04	Fe(1)-Fe(1): 3.07 – 4.06
Fe(1)-Fe(2): 4.61 – 6.36	Fe(1)-Fe(1): 4.63 – 6.40
Fe-Al: 2.21 – 2.64	Fe-Al: 2.45 – 2.66
Pr-Al: 3.09 – 3.36	La-Al: 3.13 – 3.20

ground state. However, through magnetization measurements we observe magnetic order in the Pr-lattice which is also supported by specific heat data and analysis. A crystal field quasi-doublet for Pr^{3+} at low temperature could be deduced in this compound.

II. EXPERIMENTAL DETAILS

Polycrystalline samples of PrFe_2Al_8 were prepared using arc melting method starting with high purity elements Pr (4N), Fe (3N) and Al (5N). The melting of stoichiometric amounts of materials were carried out in the water-cooled Cu-hearth of a Edmund Buehler furnace in static Argon atmosphere. A Zr-getter trap was used for purifying the Ar gas. The melted samples were annealed at 900 $^\circ\text{C}$ for 14 days. Powder x ray diffraction patterns were recorded using a Philips X'pert diffractometer which employed $\text{Cu-K}\alpha$ radiation. Magnetic properties were measured in the temperature range of 2 – 300 K using a Magnetic Property Measurement System (Quantum Design Inc. San Diego), in which magnetization in the zero field cooled (ZFC) and field cooled (FC) cycles, magnetic hysteresis and ac susceptibility were measured. Specific heat was measured in the temperature range 2 – 300 K using a commercial Physical Property Measurement System (also Quantum Design).

III. RESULTS AND DISCUSSION

A. Crystal structure

The experimentally obtained powder x ray diffraction pattern of PrFe_2Al_8 , shown in Fig. 2 (a), was refined in the orthorhombic space group $Pbam$. The structural parameters of PrCo_2Al_8 [11] were used as the starting model for the Rietveld refinement [14] using FullProf software[15]. The results of the refinement procedure are presented in (a) as solid lines along with the allowed Bragg peaks (vertical ticks) and the difference pattern (dotted line). The refined atomic and lattice parameters are collected in Table I. In Fig. 2 (b), the diffraction pattern of LaFe_2Al_8 is presented along with the results

of Rietveld fit. A comparison of the different bond distances of both the compounds are collected in Table II. The typical Pr–Al distances in PrFe_2Al_8 are found to be in the range of 3.09 \AA to 3.36 \AA , which is comparable to the distances observed for the Eu-pentagonal prism in EuRh_2Ga_8 [5]. The Pr–Pr distances are found to be in the range 4.04 \AA to 7.55 \AA . The Fe atoms have two crystallographic positions Fe(1) and Fe(2). The Fe(1)–Fe(1) distances are in the range 4.04 \AA to 6.18 \AA and the Fe(2)–Fe(2) distances are 3.06 \AA to 4.04 \AA . The Fe–Al distances are 2.21 \AA to 2.64 \AA . These distances are comparable to those found in LaFe_2Al_8 except for the larger La–La distances. In the case of CeFe_2Al_8 , the Fe(1)–Fe(1) and the Fe(2)–Fe(2) distances were reported to be 7.6 and 2.8 \AA respectively[6]. Given that the Fe–Fe distances in PrFe_2Al_8 and LaFe_2Al_8 are large and that they are separated by the Al-network, it is unlikely that the Fe-lattice would have direct magnetic exchange to lead to the development of long-range magnetic order. A careful comparison and correlation of the structural details like bond distances and Fe–Fe separation in Pr-based 1:2:8 compounds with the observed magnetic properties is very much called for.

B. Magnetic properties

The magnetic response, $M(T)$, of PrFe_2Al_8 is plotted in Fig. 3 (a) where the ZFC/FC curves of magnetization at applied field of 500 Oe are presented. Two anomalies can be clearly distinguished in the magnetic response. As temperature is decreased from 300 K, the first anomaly is observed as a shoulder-like feature at $T_{anom} \approx 34$ K while the second one manifests as a sharp peak at $T_N^{Pr} \approx 4$ K. Here we tentatively argue that the latter anomaly pertains to the magnetic

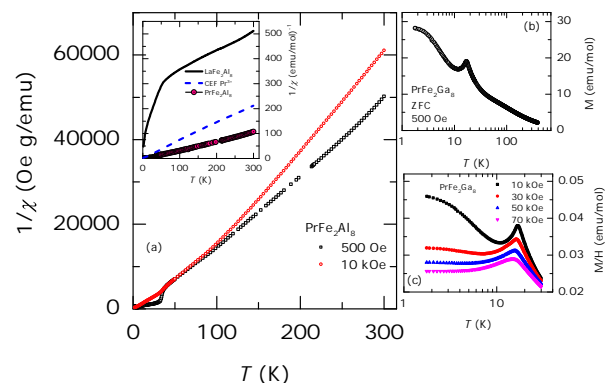


FIG. 4: (a) The inverse magnetic susceptibility, $1/\chi(T)$, of PrFe_2Al_8 plotted for two different applied fields 500 Oe and 10 kOe. The $1/\chi(T)$ plots are non-linear and the two curves do not scale suggesting magnetic correlations in the Fe lattice. In the inset, the $1/\chi(T)$ of PrFe_2Al_8 is plotted along with that of LaFe_2Al_8 . Also shown is the theoretically estimated CEF contribution to total magnetic susceptibility of PrFe_2Al_8 . (b) The magnetization curve of isostructural and isoelectronic compound PrFe_2Ga_8 shows only one magnetic transition at ≈ 15 K. The effect of applied magnetic field is to shift the peak towards lower temperature however the peak is not diminished in strength as can be seen from (c).

phase transition occurring in the Pr sublattice. The anomaly at T_{anom} could be due to short-range ordering in the Fe sublattice or even due to an impurity phase which was not detectable in the x ray diffraction data. A weak bifurcation between the ZFC and the FC curves is observed immediately close to the T_{anom} . Also shown in (a) is the plot of magnetization of the isostructural and non-magnetic analogue LaFe_2Al_8 , in which Fe is in principle the only magnetic species, which displays no magnetic transition in the temperature range 2–300 K. On the other hand, PrCo_2Al_8 displayed a magnetic transition at $T_N \approx 5$ K where Pr enters a magnetically long-range ordered state[11]. No signature of magnetism of the Co-lattice was observed. Similar absence of magnetism of the transition metal was reported in the case of CeFe_2Al_8 where intermediate valence of Ce ion leading to valence-fluctuation scenario was proposed[6]. Through neutron powder diffraction and magnetic studies clustering of the Fe ions in CeFe_2Al_8 was suggested[6]. The structural similarity and comparable interatomic distances of Fe–Fe of PrFe_2Al_8 to other 1:2:8 compounds (LaFe_2Al_8 , PrCo_2Al_8 etc) might lead to an assumption that the Fe-lattice remains non-magnetic in PrFe_2Al_8 .

Figure 3 (b) shows the results of field-scans of magnetization, $M(H)$, performed at 2 K and at 15 K. At 2 K, a ferromagnetic-like saturation of magnetization is obtained for PrFe_2Al_8 . The maximum moment attained is $M_{max}^{50 \text{ kOe}} \approx 3 \mu_B$ which is diminished compared to the full ferromagnetic moment of free ion Pr^{3+} ($3.58 \mu_B$). This indicates that the Pr-magnetic lattice does not attain complete ferromagnetic polarization at 2 K. The reduction in magnetic moment might result from short-range magnetism or cluster formation happening in the Fe sub-lattice, due to minor impurity effects in the polycrystalline sample or because of the Fe moments anti-aligning once the Pr moments start to order magnetically. In the low-field region of the magnetic hysteresis at 2 K, a sharp step-like feature is observed in PrFe_2Al_8 (inset of Fig. 3 (b)). This is reminiscent of the metamagnetic steps observed in PrCo_2Al_8 at a critical field of 0.9 T at 1.7 K[11]. The inset also displays the magnetic hysteresis obtained in field-cooled

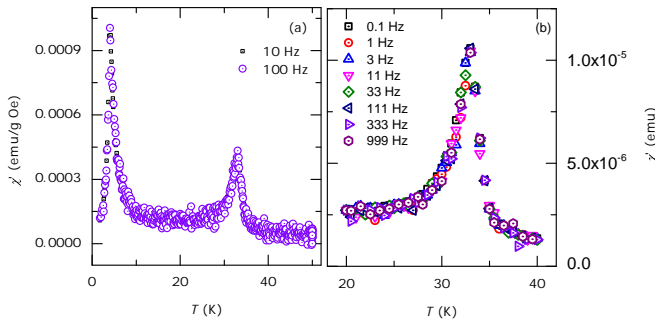


FIG. 5: (a) The real part of the ac susceptibility, $\chi'(T)$, in the temperature range 2 – 60 K showing anomalies at T_{anom} and T_N^{Pr} with applied frequencies 10 Hz and 100 Hz. (b) The $\chi'(T)$ at T_{anom} is measured for wider range of frequencies, 0.1 – 1000 Hz, in order to probe the magnetic ordering in detail. Neither transition displays frequency-dependent shift of the peak thereby ruling out any dynamic short-range magnetic order.

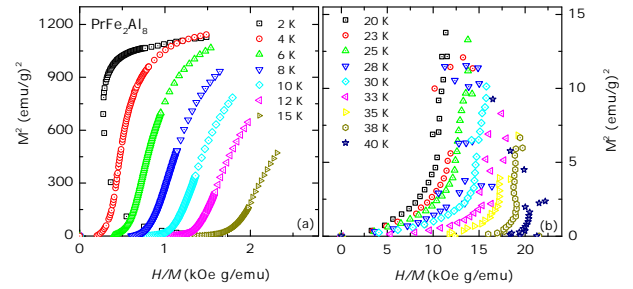


FIG. 6: (a) The Arrott plots of PrFe_2Al_8 derived from the magnetization isotherms between 2 K and 15 K which covers the temperature range around T_{N2} . The Arrott plots for the range 20 K to 40 K across T_{anom} is shown in (b). No signature of spontaneous ferromagnetism is observed in either cases however, (b) matches with the case of a disordered ferromagnet.

(at 5000 Oe) conditions at 2 K. A shift of the hysteresis loop is present as seen in the inset of (b). Though a weak feature, this hints at an inherent exchange bias-like effect in PrFe_2Al_8 [16]. Field-cooling the sample in 5000 Oe did not lead to an enhancement of maximum moment value attained at 2 K. The magnetization isotherm at 15 K does not present a magnetic hysteresis loop or any other features typical of a ferromagnet (see Fig. 3 (b)). In Fig. 3 (c), the zero field-cooled magnetization curves obtained on PrFe_2Al_8 with different applied fields (800 Oe to 20 kOe) are plotted together as M_{ZFC}/H . It can be seen that the magnetic transition at T_N^{Pr} is suppressed, however, the anomaly at T_{anom} is robust against 20 kOe. The peaks of the transitions are seen to remain without any significant shift upon the application of magnetic field.

Fig. 4 (a) shows the inverse magnetic susceptibility, $1/\chi(T)$, of PrFe_2Al_8 plotted for two values of applied magnetic fields *viz.*, 500 Oe and 10 kOe. A fit to the data assuming ideal Curie-Weiss behaviour was not possible due to the nonlinear behaviour of $1/\chi(T)$ especially at elevated temperatures. The non-linearity is attributed to crystalline electric field (CEF) effects of Pr. From (a) it is clear that the $1/\chi(T)$ curves for different applied magnetic fields do not scale with each other. This feature is a strong indicator to the presence of short-range magnetic correlations in the Fe-lattice. Curie-Weiss fit performed on the $1/\chi(T)$ data of LaFe_2Al_8 (presented in Fig. 4) resulted in a effective moment of $\approx 3 \mu_B$. A very high Curie-Weiss temperature, $\theta_{cw} \approx -285$ K was obtained for LaFe_2Al_8 which suggests prominent antiferromagnetic correlations obviously stemming from the short-range correlations of the Fe subsystem. On the other hand, the non-Fe compound PrCo_2Al_8 is reported to display a linear $1/\chi(T)$ with a perfect Curie-Weiss behaviour and no magnetic contribution from Co[11]. The only magnetic ordering in PrCo_2Al_8 was detected in the Pr lattice. In order to disentangle the magnetism of Pr and Fe in PrFe_2Al_8 , a rough estimate of the van Vleck contribution due to Pr^{3+} was theoretically calculated using the software McPhase[17] assuming the Pr^{3+} crystalline electric field environment in *Pbam*. The theoretically estimated $1/\chi(T)$ is plotted as a dashed-dotted line in the inset of Fig. 4. From this figure it is clear that in both PrFe_2Al_8 and

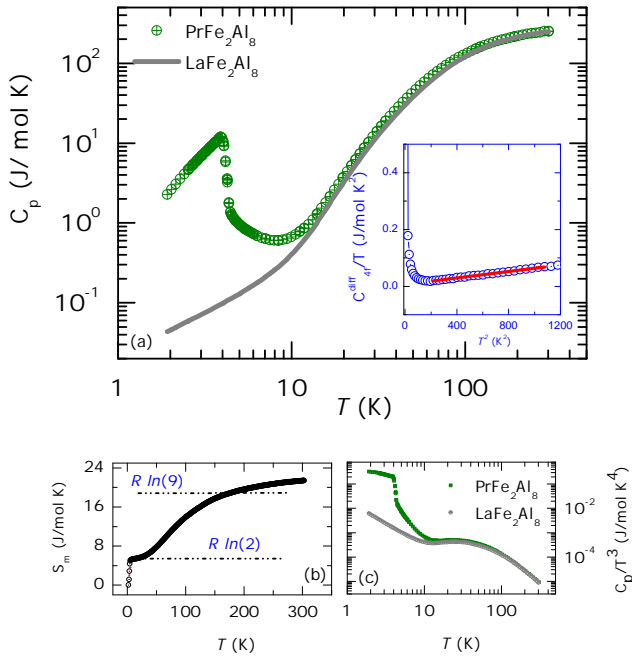


FIG. 7: (a) The specific heat, $C_p(T)$, of PrFe_2Al_8 is presented in circles. The phase transition at $T_{N2} \approx 4$ K is evident. The solid line is the $C_p(T)$ of the non-magnetic analogue, LaFe_2Al_8 . The inset shows the plot of C_{4f}^{diff}/T versus T^2 (circles) and the linear fit (solid line) to obtain γ . (b) Shows the magnetic entropy, $S_m(T)$ which attains $R \ln(2)$ at T_{N2} . (c) Shows the plot of C_p/T^3 versus T to expose the presence of phonon modes.

LaFe_2Al_8 , short-range correlation of Fe is present till elevated temperatures.

As a means to understand the multiple magnetic ordering taking place in PrFe_2Al_8 , the magnetic properties of isostructural, isoelectronic compound PrFe_2Ga_8 were also recorded. Those are presented in Fig. 4 (b) and (c). PrFe_2Ga_8 presents only one magnetic transition at ≈ 15 K. At very low temperatures close to 2 K, a saturation-like effect is discernible which hints at possible imminent magnetic ordering phenomena. The effect of applied magnetic fields on the transition temperatures is probed and the data is presented in (c). It is observed that the peak at 15 K shifts to low temperatures upon application of magnetic field. This suggests the antiferromagnetic nature of the phase transition.

Fig. 5 (a) shows the real part of ac susceptibility, $\chi'(T)$, measured at 10 Hz and at 100 Hz. Both the anomalies T_{anom} and T_N^{Pr} are reproduced. However, the ac susceptibility data do not present any frequency-dispersion for the peaks. In order to confirm the nature of the peak at T_{anom} , $\chi'(T)$ was measured at more number of frequencies as shown in (b). However, very feeble frequency dependence of the peak was observed (from 32.99 K for 0.1 Hz to 33.50 K for 999 Hz) which did not conform to response from spin glass-like clusters. Hence, if at all short-range static or dynamic magnetism arising from Fe-lattice is present in the sample of PrFe_2Al_8 , it remains masked by the long-range magnetism of Pr. Microscopic probes of magnetism like Mößbauer spectroscopy,

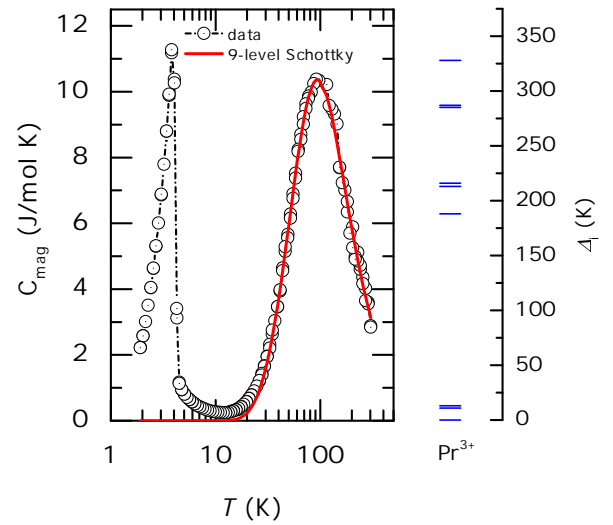


FIG. 8: The magnetic part C_{mag} of PrFe_2Al_8 is shown in black circles in a semi-log plot. The magnetic phase transition at T_{N2} is clearly visible as a sharp peak. A Schottky-like peak is observed as centred at ≈ 70 K which is modelled by assuming a 9-level energy scheme [Eqn. (1)]. The estimated CEF energy levels, Δ_i , are shown.

NMR or μSR are required to extract the Fe-magnetism in this case. As a final step in the analysis of the nature of magnetism at T_N^{Pr} , Arrott plots are presented in Fig. 6 which is derived from the magnetization isotherms in the range 2 K to 15 K. Notably, the low temperature curves do not support a pure ferromagnetic feature where the Arrott plots ought to be straight lines[18]. Instead, an "S"-like curvature is present in (a) which could suggest first-order-like nature or inhomogeneous magnetism. In the case of (b), a close similarity with the case of a disordered ferromagnet is apparent[18].

C. Specific heat

The experimentally measured heat capacity, $C_p(T)$, of PrFe_2Al_8 is presented in Fig. 7 (a) plotted as circles. A clear peak in $C_p(T)$ signifying the phase transition at $T_N^{Pr} \approx 4$ K is observed. As a non-magnetic reference, the $C_p(T)$ of LaFe_2Al_8 is presented in (a) as a solid line. The low temperature part of the specific heat is plotted as C_{4f}^{diff}/T versus T^2 where, $C_{4f}^{\text{diff}} = (C_p(\text{Pr}) - C_p(\text{La}))$ in the inset of (a) along with the linear fit (red solid line) which estimated the Sommerfeld coefficient, $\gamma_{4f} \approx 6$ mJ/mol-K². It is to be noted that the value, γ_{4f} that we have obtained is through a subtraction procedure and actually assumes comparable lattice specific heats for the Pr and La compounds. The overall feature of the C_p/T versus T^2 in the present case is similar to that of EuRh_2In_8 where a transition at 5 K occurs first and further low in temperature, a broad anomaly occurs at 1.6 K [5]. The magnetic specific heat obtained by subtracting the $C_p(T)$ of LaFe_2Al_8 from that of PrFe_2Al_8 displays a very broad peak centered at approximately 70 K (shown later in Fig. 8). The latter peak might arise from the crystal field levels of Pr^{3+} . The mag-

TABLE III: The peculiarities of magnetic ordering in different PrT_2X_8 compounds are collected. SRO = short-range order. LRO = long-range order.

PrT_2X_8	Pr-ordering	T-ordering
PrFe_2Al_8	4 K (LRO)	SRO may be present
PrCo_2Al_8	5 K (LRO)	not observed down to 2 K
PrFe_2Ga_8	15 K (LRO)	SRO may be present
PrCo_2Ga_8	not observed down to 2 K	not observed down to 2 K

netic entropy, S_m , estimated through numerical integration of the magnetic specific heat is presented in Fig. 7 (b). Assuming the presence of Pr^{3+} ($J = 4$), the theoretical value of $S_m = R \ln(2J + 1)$ is ≈ 18 J/mol K. At about 180 K this entropy is recovered while only about 40% of this value is attained at close to the magnetic transition at T_N^{Pr} . In Fig. 7 (b), S_m attains a value of $R \ln(2)$ at T_N^{Pr} thereby confirming a doublet state for Pr^{3+} . This observation together with the low and normal-metal value of 6 mJ/mol K² for the Sommerfeld coefficient show that the magnetic ordering at T_N^{Pr} in PrFe_2Al_8 involves well-localized magnetic moments of Pr^{3+} ion. In the panel (c), a plot of C_p/T^3 versus T is shown which brings out the phononic contribution in this compound. Such a plot would exhibit a sizeable peak at T_{max} if significant contribution from optical phonons is present. In the present case, T_{max} is quite broad and centred roughly around 30 K. For a comparison, the plot of LaFe_2Al_8 is also present which exhibited a similar feature while CeFe_2Al_8 and CeCo_2Al_8 did not[7].

The magnetic part of the specific heat obtained by subtracting the specific heat of LaFe_2Al_8 from that of PrFe_2Al_8 was used to analyze the crystalline electric field (CEF) levels of Pr^{3+} ion. In the given symmetry of the space group $Pb\bar{3}m$, the Pr ion is situated at the Wyckoff position of $4g$ which has a point symmetry m . In this orthorhombic crystal field environment, Pr^{3+} with $J = 4$ would possess 9 singlet levels. The multilevel Schottky expression for a 3H_4 system with nine singlet levels is written as:

$$C_p^{CEF} = k_B \left[\sum_{i=1}^9 \left(\frac{\Delta_i}{k_B T} \right)^2 p_i - \sum_{i=1}^9 \left(\frac{\Delta_i p_i}{k_B T} \right)^2 \right] \quad (1)$$

where $p_i = Z^{-1} \exp(-\Delta_i/k_B T)$ is the Boltzmann population factor, $Z = \sum_i \exp(-\Delta_i/k_B T)$ is the partition function, k_B is the Boltzmann constant and Δ_i are the locations of the CEF energy levels above zero. A starting point for the crystal field energy-level values were obtained by modelling the case of Pr^{3+} in PrFe_2Al_8 using a point-charge model employing the software McPhase and the subroutine solion[17]. The energy-level values obtained using this method were used in the above expression in order to perform a least-squares fit of the magnetic specific heat data shown in Fig. 8. Since the values of Δ_i from inelastic neutron scattering experiments are not available for PrFe_2Al_8 or closely related systems, tentative initial values were instead obtained from the reports on 1:1:3 systems PrGaO_3 [19] and PrIrSi_3 [20]. A curve fit to the experimental data following Eqn (1) is presented in Fig. 8 and the estimated CEF energy levels, Δ_i , are also shown. It must be noted that

an accurate estimation of the CEF levels, Δ_i , is best possible through inelastic neutron scattering methods and usually the Schottky contribution to the specific heat is calculated using the Δ_i thus derived[20]. The amorphous ferromagnetic contribution from the Fe sub-lattice would have very little contribution towards the total magnetic entropy however the exchange field generated this way may polarize the low-lying crystal field levels. The magnetic entropy plotted in Fig. 7 (c) clearly shows full doublet close to T_N^{Pr} whereas the CEF analysis shows the first two excited energy levels at approximately 10 K. An almost full occupation of 9 levels is attained at ≈ 200 K in Fig. 7 (c) whereas the CEF analysis presents highest level at above 300 K. These qualitative inconsistencies might have their origin in the subtraction procedure performed to obtain the magnetic specific heat, or inaccuracies in the estimation of crystal field levels. The distinct feature in $S_m(T)$ at T_N^{Pr} however is unequivocal and reproducible regardless of whether $C_p(T)$ or $C_{4f}(T)$ is inspected for the entropy change at T_N^{Pr} . Alternatively, the itinerant electron magnetism inherent to the material also can contribute towards such a feature. Keeping in mind that a faithful estimation of the CEF levels are possible through inelastic neutron scattering methods, our future endeavour would be to carry out an accurate estimation of the CEF levels.

IV. DISCUSSION

The magnetic properties exhibited by PrT_2X_8 compounds calls for deeper investigations involving microscopic structural probes like neutrons and μSR . The structural peculiarities comprising of the quasi cage-like structure of Al polyhedra and the strand-like alignment of Pr and T along the c -axis are of key significance. Among the various RT_2X_8 compounds investigated, the Ce-based compounds CeFe_2Al_8 and CeCo_2Al_8 displayed no signature of magnetic ordering down to 0.4 K [7]. These compounds were investigated for the strongly correlated electron behaviour. In CeCo_2Al_8 , a stable Ce magnetic moment was observed while in CeFe_2Al_8 , intermediate-valent states. Single crystal studies on $\text{CeCo}_{2-x}\text{M}_x\text{Al}_8$ [$M = \text{Mn, Fe, Ni}$] concluded that the $4f$ moment was not perturbed by the size of the dopant atom[12]. However, signs of ferromagnetism emerged in the case of doping with Mn and Fe. A report on neutron diffraction investigation on CeFe_2Al_8 did not reveal magnetic ordering down to 1.5 K[6] however, the magnetization and Mößbauer data suggested clusters of Fe below 6.5 K. On the other hand, PrCo_2Al_8 was found to order magnetically below 5 K[11] with a metamagnetic-like transition at a critical field of 0.9 T. Interestingly, the magnetic susceptibility was reported to adhere to ideal Curie-Weiss behaviour with an effective magnetic moment of 3.48(5) $\mu_B/\text{f.u.}$ suggesting the presence of stable Pr^{3+} moment. No contribution to magnetism from Co moment was inferred. In Table III, the magnetic properties of the Pr-based RT_2X_8 compounds are collected.

Rietveld analysis of the laboratory x ray data indicates that the Pr-based 1:2:8 compounds PrFe_2Al_8 , PrFe_2Ga_8 and PrCo_2Ga_8 belong to the same orthorhombic $Pb\bar{3}m$ space

group with similar lattice parameters and comparable interatomic distances for Pr–Pr, Fe–Fe distances (see Table II). PrCo₂Ga₈ is found to display no signs of magnetic ordering (data not presented) while PrFe₂Ga₈ shows a magnetic transition at 15 K. Given the structural similarities between these compounds, it is interesting to observe multiple magnetic anomalies in PrFe₂Al₈. Both the anomalies do not display any frequency dispersion in ac susceptibility measurements while the anomaly at 4 K is suppressed upon the application of 10 kOe magnetic field. An added proof for the Pr ordering at T_N^{Pr} is obtained from the magnetic entropy derived from total specific heat (Fig. 7) where $S_m = R \ln(2)$ is recovered at T_N^{Pr} . However, Arrott plots indicate the presence of inhomogeneous magnetism at low temperatures[18, 21]. Compared to the reported case of PrCo₂Al₈[6], the compounds of the present paper PrFe₂Al₈, PrFe₂Ga₈ and PrCo₂Ga₈ are seen to exhibit non-linear features in inverse magnetic susceptibility clearly suggesting the role played by the crystalline electric field effects. Most importantly, the $1/\chi(T)$ data of PrFe₂Al₈ presented in Fig. 4 (a) supports the role of CEF levels of Pr³⁺ as well as the presence of magnetic fluctuations of Fe which persist up to 300 K or above.

The specific heat and CEF analysis of Pr-based cubic systems are of fundamental interest to probe the resulting magnetic ground state. Several prototypical compounds have been investigated in this regard. A number of Pr-based systems show magnetic order despite a nonmagnetic ground state suggested by the CEF predictions. In fact, magnetic order can be established via the admixture of higher lying CEF levels into a ground state of higher degeneracy in the case of exchange energy larger than the first CEF excitation[22]. Such CEF assisted ferromagnetic ordering is observed in the case of PrNiGe₂[23]. On the other hand, if the exchange interactions between the rare earth ions dominate over the CEF, the magnetic moment associated with the 4*f* electrons can be completely quenched[24]. Induced magnetism in the singlet ground state system PrIrSi₃ has been observed with a surprisingly large energy splitting of 92 K [25]. Another Pr-based compound, PrAu₂Si₂ and its doped variant PrAu₂(Si_{1-x}Ge_x)₂ are systems where dynamic fluctuations of the CEF levels were found to hold the key to destabilizing the induced moment magnetism and realizing spin glass state[26, 27]. In PrPtBi, for example, Pr³⁺ occupies a cubic local symmetry which splits the ninefold degenerate ground

state of ³H₄ in to one singlet (Γ_1), one doublet (Γ_3) and two triplets (Γ_4, Γ_5)[28]. An energy separation of 87.5 K between the ground state and the first excited state was estimated.

V. CONCLUSIONS

In conclusion, we have studied the magnetic and thermodynamic properties of the intermetallic compound PrFe₂Al₈ which crystallizes in *Pbam* symmetry with quasi cage-like structure of Al atoms. The structural features of PrFe₂Al₈ resembles those of other isostructural compounds like LaFe₂Al₈ and PrCo₂Al₈. Magnetic measurements reveal two anomalies at $T_{anom} \approx 34$ K and $T_N^{Pr} \approx 4$ K. The latter anomaly is likely to originate from magnetic ordering in the Pr lattice however, a conclusion about this requires further experimental proofs. Signatures of short-range magnetic fluctuations in the Fe lattice are also obtained however, could be mediated by impurities. Metamagnetic-like steps in the magnetization isotherm at 2 K is clearly evidenced. The phase transitions at $T_N^{Pr} \approx 4$ K is also reflected in the specific heat. Analysis of magnetic entropy identifies a value of $R \ln(2)$ at 4 K suggesting the presence of a Pr doublet crystal field level in spite of the symmetry of Pr site predicting only 9 singlet levels. Neutron powder diffraction and inelastic neutron scattering experiments are called for to understand the magnetic properties and the CEF level schemes of PrFe₂Al₈.

‡Present address: Department of Applied Physics, Birla Institute of Technology, Mesra, Ranchi, Jharkhand, India

Acknowledgements

H. S. N. and R. K. K. acknowledge Manh Duc Le for help with the McPhase software and CEF calculations. They also thank the FRC/URC for a postdoctoral fellowship. A. M. S. thanks the SA-NRF (93549) and the FRC/URC of UJ for financial assistance.

-
- [1] M. D. Koterlin, B. S. Morokhivskii, R. V. Lapunova, and S. O. M., Sov. Phys.-Solid State **31**, 1826 (1989).
 [2] R. Pöttgen and D. Kußmann, Z. Anorg. Allg. Chem. **627**, 55 (2001).
 [3] R. E. Galdishevskii, Y. P. Yarmolyuk, and Y. N. Grin, Sov. Phys. Crystallogr. **28**, 641 (1983).
 [4] J. D. Thompson, Physica B **329**, 446 (2003).
 [5] V. Fritsch, S. Bobev, N. O. Moreno, Z. Fisk, J. D. Thompson, and J. L. Sarrao, Phys. Rev. B **70**, 052410 (2004).
 [6] M. Kolenda, M. D. Koterlin, M. Hofmann, B. Penc, A. Szytuła, A. Zygmunt, and J. Zukrowski, J. Alloys and Comp. **327**, 21 (2001).
 [7] S. Ghosh and A. M. Strydom, Acta Phys. Polon. Ser. A **121**, 1082 (2012).
 [8] K. Momma and F. Izumi, J. Appl. Cryst. **41**, 653 (2008).
 [9] J. H. Van Vleck, Rev. Mod. Phys. **34**, 681 (1962).
 [10] O. M. Sichevich, R. V. Lapunova, Y. N. Grin, and Y. P. Yarmolyuk, Izv. Akad. Nauk. SSSR Metally **6**, 117 (1985).
 [11] O. Tougaard, D. Kaczorowski, and H. Noël, J. Solid State Chem. **178**, 3639 (2005).
 [12] L. J. Treadwell, P. Watkins-Curry, J. D. McAlpin, D. J. Rebar, J. K. Hebert, J. F. DiTusa, and J. Y. Chan, Inorg. Chem. **54**, 963

- (2014).
- [13] J. L. Snyman and A. M. Strydom, *J. Appl. Phys.* **111**, 07A943 (2012).
- [14] H. M. Rietveld, *J. Appl. Crystall.* **2**, 65 (1969).
- [15] J. Rodriguez-Carvajal, LLB, CEA-CNRS, France [<http://www.ill.eu/sites/fullprof/>] (2010).
- [16] J. Nogués and I. K. Schuller, *J. Magn. Magn. Mater.* **192**, 203 (1999).
- [17] M. Rotter, *J. Magn. Magn. Mater.* **272**, E481 (2004).
- [18] I. Yeung, R. M. Roshko, and G. Williams, *Phys. Rev. B* **34**, 3456 (1986).
- [19] A. Senyshyn, W. Schnelle, L. Vasylechko, H. Ehrenberg, and M. Berkowski, *J. Phys. Condens. Matter* **19**, 156214 (2007).
- [20] V. K. Anand, D. T. Adroja, A. Bhattacharyya, A. D. Hillier, J. W. Taylor, and A. M. Strydom, arXiv:1407.5205 (2014).
- [21] P. K. Das, A. Bhattacharyya, R. Kulkarni, S. K. Dhar, and A. Thamizhavel, *Phys. Rev. B* **89**, 134418 (2014).
- [22] B. Bleaney, in *Proc. Royal Soc. London A* (The Royal Society, 1963), vol. 276, pp. 19–27.
- [23] J. L. Snyman and A. M. Strydom, *J. Appl. Phys.* **113**, 17E135 (2013).
- [24] G. T. Trammell, *Phys. Rev.* **131**, 932 (1963).
- [25] V. K. Anand, D. T. Adroja, A. Bhattacharyya, A. D. Hillier, J. W. Taylor, and A. M. Strydom, *J. Phys.: Condens. Matter* **26**, 306001 (2014).
- [26] A. Krimmel, J. Hemberger, M. Nicklas, G. Knebel, W. Trinkl, M. Brando, V. Fritsch, A. Loidl, and E. Ressouche, *Phys. Rev. B* **59**, R6604 (1999).
- [27] E. A. Goremychkin, R. Osborn, B. D. Rainford, R. T. Macaluso, D. T. Adroja, and M. Koza, *Nat. Phys.* **4**, 766 (2008).
- [28] H. Suzuki, M. Kasaya, T. Miyazaki, Y. Nemoto, and T. Goto, *J. Phys. Soc. Jpn.* **66**, 2566 (1997).